ORIGINAL PAPER

Numerical simulation of the impact of land cover change on regional climate in China

Yong-Li Wang · Jin-Ming Feng · Hao Gao

Abstract Land use and land cover change (LUCC) can modify the physical and thermodynamic characteristics of the land surface, including surface roughness, albedo, and vegetation fraction, among others. These direct changes can result in a series of impacts on regional climate. In this paper, the simulated results over China under the scenario of LUCC using weather research and forecasting model are presented. The period for the simulation is from December 2006 to December 2011. Two experiments are initialized by the LUCC datasets derived from the MODIS data of 2001 and 2008, respectively. The results show that the LUCC in most areas of China reduces the surface albedo and increases the surface temperature. Especially in the Hetao Plain, the magnitude of increased surface temperature is above 0.5 °C in winter, and the increase in winter is more obvious than in summer. The precipitation in the Hetao Plain increases. The sensible heat in most parts of East China is reduced, while the latent heat is increased in most areas of China.

Abbreviations

LUCC	Land use and land cover change
WRF	Weather research and forecasting model
IGBP	International Geosphere Biosphere Programme
IHDP	International Human Dimensions of Global Environmental Change Programme
GIS	Geographical Information System
SST	Sea-surface temperature
TRMM	Tropical Rainfall Measuring Mission
NCAR	National Center for Atmospheric Research
ARW	Advanced Research WRF
WSM	WRF single-moment
YSU	Yonsei University
PBL	Planetary boundary layer
RRTM	Rapid radiative transfer model
EVI	Enhanced vegetation index
NASA	National Aeronautics and Space Administration
BRDF	Bidirectional reflectance distribution function
HDF	Hierarchical data format
LAI	Leaf area index
LSM	Land surface model

Y.-L. Wang · J.-M. Feng (✉)
Key Laboratory of Regional Climate-Environment for East Asia,
Institute of Atmospheric Physics, Chinese Academy of Sciences,
Beijing 100029, China
e-mail: fengjm@tea.ac.cn

H. Gao
National Satellite Meteorological Center, China Meteorological
Administration, Beijing 100081, China

Y.-L. Wang
Graduate University of the Chinese Academy of Sciences,
Beijing 100049, China

1 Introduction

In the past two centuries, human activities had great impacts on the land surface by altering the landscapes. Some previous studies suggested that 83 % of the Earth's land surface has been affected by human settlements and activities, leaving only 17 % in the wilderness (WCS & CIESIN 2002), and ultimately these changes influenced the climate as well as the Earth's land cover and hydrological cycles. Land use and land cover change (LUCC) is one of the most sensitive indicators that echo the interactions between human activities and natural environments. Therefore, LUCC has become a core issue in the global environmental change and sustainable development disciplines. Many studies for LUCC have addressed deforestation, desertification, biodiversity loss, urbanization, and the interaction between land cover and the water cycle, among others (Pielke et al. 2002; Feddema et al. 2005; Findell et al. 2007; Pitman et al. 2009). In early 1987, the Joint International LUCC Project of the International Geosphere

Biosphere Programme (IGBP) and the International Human Dimensions of Global Environmental Change Programme published a science/research plan with the goal to reveal the basic processes of interaction between the Earth's environmental systems and human production systems (agriculture, urbanization, etc.) through monitoring, interpreting, modeling, and prediction of LUCC extensively at global and regional scales (Turner et al. 1995; Nunes and Auge 1996). To monitor and understand LUCC, satellite remote sensing techniques have been widely applied to extract multi-temporal land use information (Lu et al. 2004; Shalaby and Tateishi 2007).

The land surface influences local, regional, and global climate across many time scales. Therefore, LUCC could impact land and air resources, biodiversity, water quality, radiation budgets, carbon cycling, and livelihoods. Over the last decades, a range of models for LUCC have been developed to meet the needs of land management and to better assess and project the role of LUCC in the functioning of the climate system. Several climate model simulations have shown significant sensitivities to these land surface characteristics. Chase et al. (1996) found that decreasing leaf area index (LAI) globally made the surface latent heat flux decrease and the sensible heat flux increase during January and July in their general circulation model simulations. Bonan (1997) concluded that the land use change of natural vegetation to present-day vegetation cover caused a cooling of 1 K in the eastern USA, a warming of 1 K in the western USA during spring, and a cooling of 2 K during summer over large regions of the central USA. Studies by Xue et al. (1996) and Lu and Shuttleworth (2002) found that vegetation cover could have a significant influence on predictions of surface temperature and precipitation. Thus, both spatial and temporal distributions of vegetation used in the climate models need to be sufficiently detailed. Fuller et al. (2007) examined the effect of LUCC on the distributions of 86 endemic mammal species in Mexico in the years 1970, 1976, 1993, and 2000. The authors concluded that this fauna could have been protected much more efficiently if a conservation plan had been implemented in 1970. Issiaka et al. (2012) integrated remote sensing and geographical information system to better understand LUCC influence through diachronic analysis. Terry et al. (2012) developed a scenario-based modeling framework to analyze potential future land use change in the Great Plains.

Accurate representation of land surface is important to conduct reliable and accurate numerical modeling experiments. Because different land cover types have different vegetation and land use-related parameters in the climate models, such as albedo, surface roughness, green vegetation fraction, and stomatal resistance, inaccurate or incorrect land surface data could result in large biases in regional and global climate simulations due to misrepresentation of the partitioning of available energy between sensible heat and latent heat and of precipitation between evapotranspiration

and runoff (Zhao et al. 2001). Remote sensing provides a more accurate representation of the Earth's surface on different spatial and temporal scales and is therefore an attractive source for creating land cover data as model's initial field. The recent availability of multiple high-quality Moderate Resolution Imaging Spectro-radiometer (MODIS) land data is used to investigate the global and regional effects of a new land surface data set on land surface variables in Common Land Model (Tian et al. 2004). LaCasse et al. (2008) studied the impacts of high-resolution (1 km) MODIS-derived sea-surface temperature (SST) field on the overlying marine atmospheric boundary layer thermodynamic and kinematic structures using the Weather Research and Forecast (WRF) simulation at 2-km resolution over the Florida Peninsula. Their results showed that the use of MODIS SST composites results in enhanced convergence zones, earlier and more intense horizontal convective rolls, and an increase in precipitation as well as a change in precipitation location. Many of the cited studies highlighted the challenges involved in quantifying the impacts of the land surface conditions in numerical simulation. A missing component of these community-wide studies is the rigorous evaluation of the actual impacts of high-resolution land representation on the simulation results, especially on the general circulation.

In this study, with these above-mentioned issues in mind, the 500-m resolution MODIS for land surface initialization is used to examine the sensitivity of simulation results and possible improvements brought by the dataset. Both the traditional station-observed temperature and the Tropical Rainfall Measuring Mission (TRMM) precipitation will be used for the verification of model results. The remainder of this paper is organized as follows. "Section 2" contains a description of the WRF configuration and experiment design and the introduction of the MODIS data. Results are presented in "Section 3", followed by conclusions and discussion in "Section 4".

2 Model description and experiment design

The present study uses the National Center for Atmospheric Research WRF model with Advanced Research WRF dynamic core (version 3.2.1.). The model is configured with 28 vertical layers from the surface to 50 hPa. The other settings for physical schemes include: WRF Single-Moment (WSM) 6-class graupel scheme for microphysics (Hong and Lim 2006), the Yonsei University scheme for Planetary Boundary Layer (Hong et al. 2006), the Kain–Fritsch (new Eta) scheme for cumulus parameterization (Kain 2004), the Dudhia short-wave radiation scheme (Dudhia 1989), the Rapid Radiative Transfer Model for the longwave radiation (Mlawer et al. 1997), and the Noah land surface model (Chen and Dudhia 2001).

The National Center for Environmental Prediction final analysis data at 1×1 horizontal resolution and six-hourly is used for the initial and lateral boundary conditions. The evaluation period is from 1 December 2006 to 31 December 2011. The model outputs at every 6 h are used for analysis. The results of the WRF simulation from the cited two experiments are compared with observations.

The MODIS global land cover products over the period of 2001–2009 are derived with the enhanced spectral information from the MODIS sensor onboard the NASA Terra and Aqua satellites. The land cover datasets are produced over thousands of training samples, interpreted from high-resolution imagery at an approximate spatial resolution of 500 m (MCD12Q1) using a decision tree classifier with a supervised classification approach. The data inputs for the algorithm include MODIS surface reflectance (Channels 1–7), the enhanced vegetation index, spatial texture, land surface temperature, MODIS adjusted bidirectional reflectance distribution function, snow, elevation, and other ancillary data (Friedl et al. 2002, 2010). The classification combines prior and posterior probabilities to assign the most probable class for each location on the globe (Friedl et al. 2002). The land cover product primarily used the classification system of five land cover types, which include the IGBP classification scheme. The overall accuracy of IGBP layer is 75–80 % at the global level, 70–85 % at the continental level, and 60–95 % at the individual class level, validated by Hodges (2002) with field references.

The data are available in hierarchical data format, which are downloaded freely from the Land Processes Distributed Active Archive Center (https://lpdaac.usgs.gov/lpdaac/products) as tiles in a sinusoidal projection. The tiles are mosaicked together and re-projected as the Lambert Conformal Conic projection with map datum WGS84 at a spatial resolution of 500 m using the MODIS re-projection Tool 4.0. The datasets are clipped to the coverage of the WRF domain, and the percentage of each land cover class at each grid is calculated according to the spatial resolution in the WRF domain.

Two experiments are carried out. The only difference between the two experiments is the initial time of land use/cover. The influence of the LUCC on climate change in China is evaluated by two WRF experiments, Exp1 (2001 LUCC) and Exp2 (2008 LUCC), using the MODIS satellite data.

3 Results

In this section, we describe the land use/cover change in China first and then compare the simulated temperature and precipitation with the observations. We also show regional statistical characteristics of temperature and precipitation changes due to the LUCC. Finally, we analyze the change of surface air temperature, surface energy balance, precipitation, and low-level circulation due to the LUCC.

4 Land use and land cover change from 2001 to 2008

LUCC can affect the regional climate by changing the partitioning of available energy between sensible heat and latent heat and by changing the partitioning of precipitation between evapotranspiration and runoff (Zhao et al. 2001). Figure 1 depicts the distribution of the land cover in 2001 (Fig. 1a) and 2008 (Fig. 1b). The most obviously changed area in China is the Hetao Plain, where the shrubland had been replaced by the grassland. Based on the changes of land use/cover listed in Table 1, on all the values averaged over China, the most obviously increased vegetation is the grassland with the increased value of 3 %, and the closed and open shrublands are all decreased obviously. Based on the interdecadal trend over the central part of North China (Ma 2007), there was a drying trend that dominated east of 100° E and north of 35° N, and the most significant drying trends were manifested in the eastern part of Northwest China, the central part of North China, the central and southeastern parts of Northeast China. Overall, the precipitation may be the key
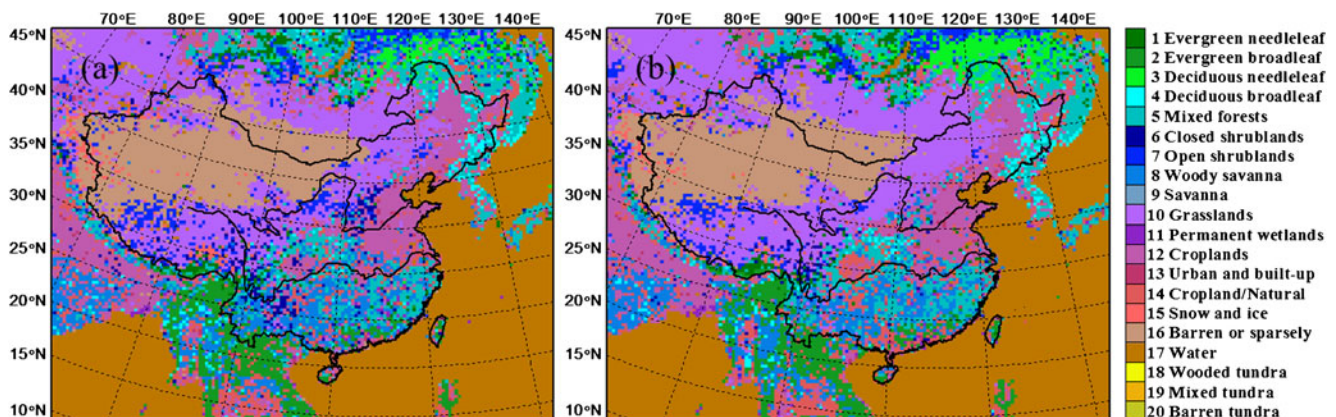

Fig. 1 Distribution of land cover 2001 (a) and 2008 (b) over the domain

Table 1 Percentage for every land use type from MODIS data of 2001 and 2008

Classification	2001	2008
Water	0.7	0.7
Evergreen needleleaf	1.2	1.4
Evergreen broadleaf	1.5	1.9
Deciduous needleleaf	0.4	0.7
Deciduous broadleaf	1.8	1.8
Mixed forests	9.5	9.9
Closed shrublands	3.0	1.2
Open shrublands	4.8	3.6
Woody savannas	7.4	7.1
Savannas	0.2	0.0
Grasslands	21.0	24.0
Permanent wetlands	0.4	0.3
Croplands	15.7	14.8
Urban and built-up	0.9	0.9
Cropland/natural	4.7	7.0
Snow and ice	1.1	0.7
Barren or sparsely	25.6	24.1

factor, which led to the transition from open shrubland and closed shrubland to the grassland.

5 Validation of temperature and precipitation

Comparisons between the observed and WRF-simulated annual average temperature and summer mean precipitation are performed. A climatological monthly mean data of air temperature comes from 720 stations in China, and the precipitation is based on the TRMM data. The TRMM is a joint endeavor between the NASA and Japan's National Space Development Agency. It was designed to monitor and study tropical rainfall and the associated release of energy that helps to power the global atmospheric circulation, which shapes both global weather and climate.

The Exp1 results are used as the simulated ones to compare with the observed data. Figure 2a, b shows the spatial patterns of the observed and simulated annual average temperature. They indicate that the model temperature distribution is basically consistent with the observation, and there are low-temperature areas in the Yangtze River Basin and South China. Figure 2c, d
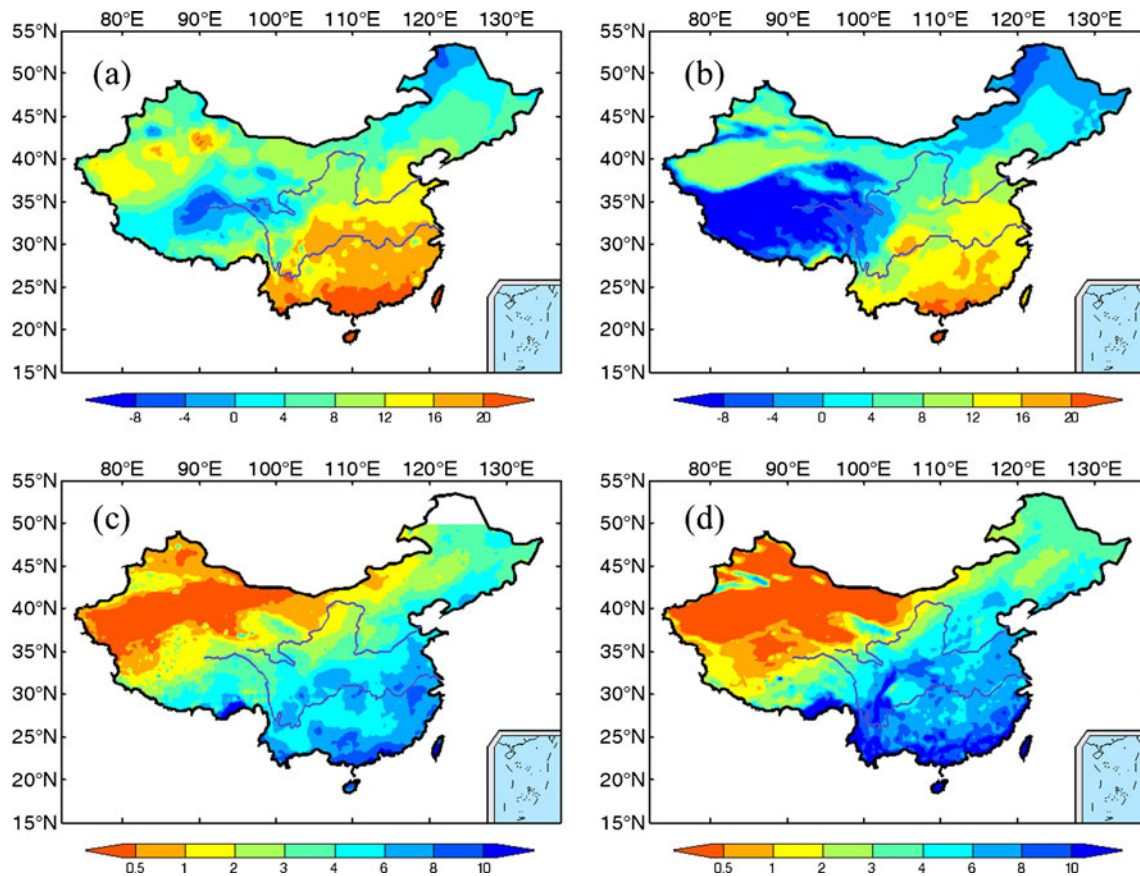

Fig. 2 Comparison of annual mean temperature (°C) and summertime mean precipitation (mm/day) between the observation and the simulation: **a** observed temperature, **b** simulated temperature, **c** observed precipitation, and **d** simulated precipitation

shows the spatial patterns of observed and simulated precipitation over the model domain. In general, the model is capable of reproducing the spatial distribution of the observed precipitation. The observed precipitation pattern (Fig. 2c) is characterized by less precipitation in the North and more precipitation in the Yangtze River Basin and South China. Overall, the model precipitation captures the patterns and magnitudes over most parts of China fairly well (Fig. 2d). The precipitation in the Yangtze River Basin and South China is overestimated.

6 Regional statistical characteristics of temperature and precipitation change

Comparing the spatial distributions of land use/cover in 2001 and 2008, one could see different climatic characteristics in China. Therefore, to study the effects of climate change in different areas with different climates, three typical sub-regions are chosen (Fig. 3a): the Hetao Plain, the Yangtze River Delta, and the Pearl River Delta. The Yangtze River Delta and the Pearl River Delta are located in the plains. However, the Hetao Plain is mainly located north of the Loess Plateau and belongs to an arid and semi-arid region, which is a place with the most significant land use/cover change in China in recent years. The Yangtze River Delta and Pearl River Delta are both influenced by the strong East Asian monsoon, which brings rich rainfall and high temperature in summer. The differences (Exp2 minus Exp1) of mean temperature (Fig. 3b) and precipitation percentages (Fig. 3c) for the three sub-regions' averages are also calculated. Here the precipitation percentage is the difference between Exp1 and Exp2 with respect to Exp1. From the figures, it is obvious that all the temperature and precipitation percentage increased in China, including the Yangtze River Delta and Pearl River Delta. The temperature in the Hetao Plain had the most significant increase, and precipitation had a great increase in the Yangtze River Delta. Figure 4 gives the monthly changes of temperature and precipitation percentage of 2007–2011 due to the LUCC in each region. One can see that the temperature and precipitation in the whole China increased. Similar temperature change can be seen in the Hetao Plain, but the LUCC only had great impact on the precipitation in summer. The LUCC had a dominating influence on temperature over the Pearl River Delta and the Yangtze River Delta; it played a different leading role in the temperature of summer and other seasons in the Yangtze River Delta. One could also see that the LUCC had a significant influence on the rainfall in the summer and autumn in the Yangtze River Delta and in the Pearl River Delta.

7 Analyses of surface air temperature and surface energy balance

Figure 5a, c shows the spatial distributions of surface temperature in Exp1 for summer and winter, respectively, while Fig. 5b, d shows the differences (Exp2 minus Exp1) to reflect the
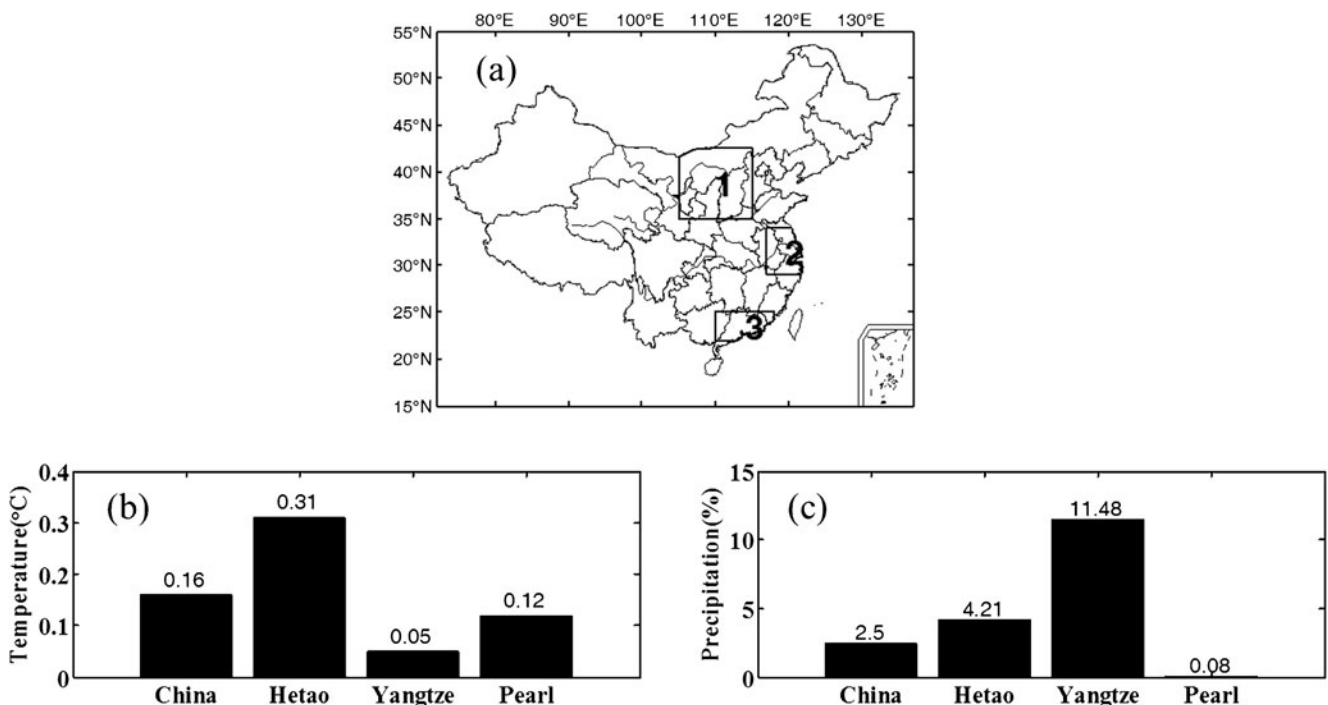

Fig. 3 Region division (a 1 the Hetao Plain, 2 Yangtze River Delta, 3 Pearl River Delta) and annual mean temperature change (b, °C) and precipitation change (c, %) due to LUCC
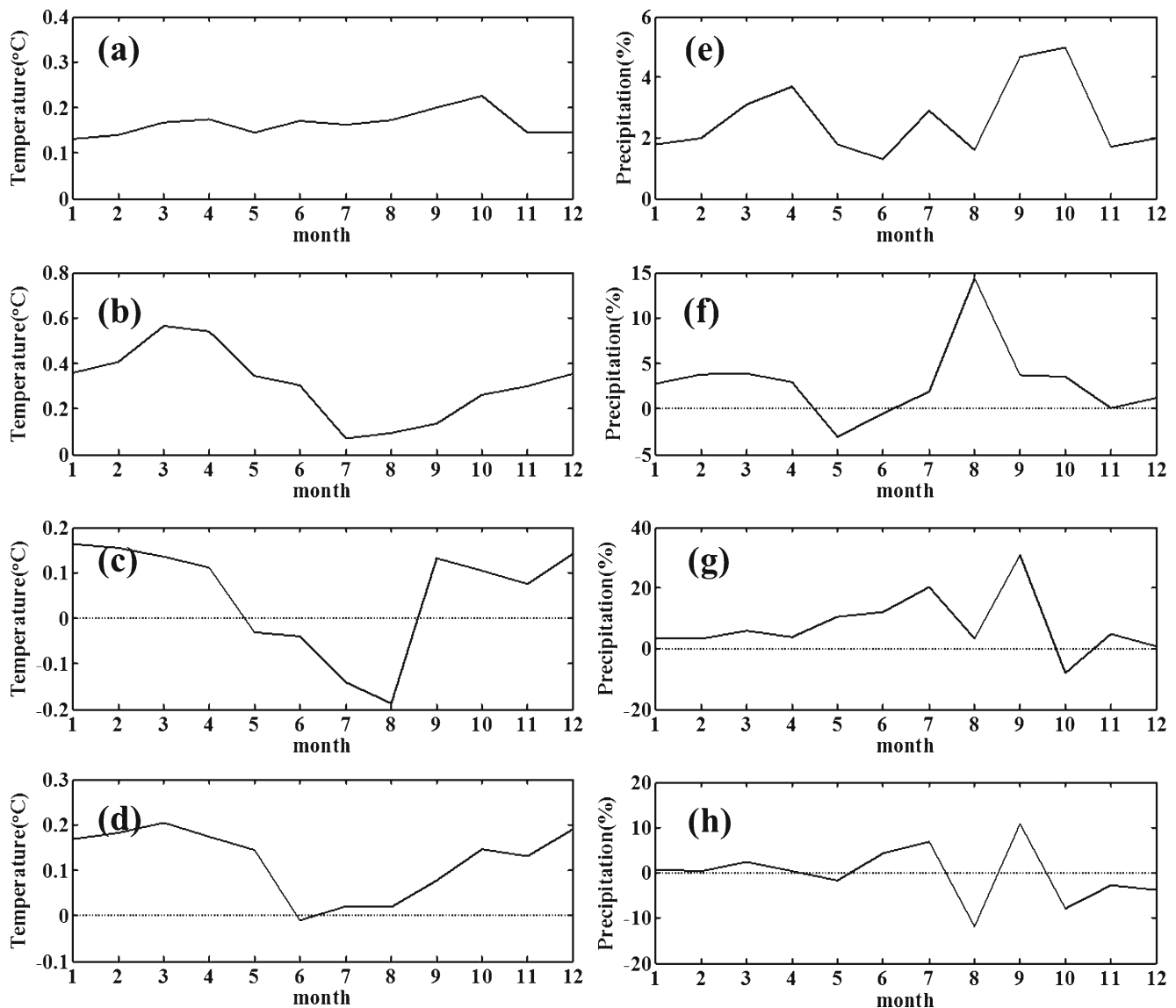
Fig. 4 Monthly variations of temperature change (*left panels*, °C) and precipitation change (*right panels*, %) of the 5 years due to LUCC averaged over each region: **a**, **e** China, **b**, **f** the Hetao Plain, **c**, **g** the Yangtze River Delta, and **d**, **h** the Pearl River Delta

influence of LUCC in summer and winter, respectively. The summer spatial distribution of temperature indicates that the most obvious increase of summer temperature was in the north and south part of Hetao Plain, with a magnitude of change above 0.35 °C. The most noticeable decrease was located in Yangtze River Basin. Unlike the change of summer temperature, the winter temperature increased in most parts of east China, and the most obvious place of change appeared in the Hetao Plain and the north of it, with an amplitude above 0.5 °C. All of these show that the temperature changes are dominated by near-surface changes in land cover. The characteristics of land surface can affect the temperature and humidity levels in the lower atmosphere. The *t*-test values which are absolute values in four different confident levels (70, 80, 90, and 95 %) (Fig. 5c, f) indicate that the areas were with added 0.5 °C almost all through the 90 % confidence level.

Surface albedo is an important parameter in land surface process, the climate system, and the radiation transport. Surface albedo could be affected by the underlying surface type, vegetation cover, angle, and spectral distribution of incident solar radiation, atmospheric conditions, geomorphology, mineral materials, surface roughness, and many other factors. With more intensified human activities, there has been a major change of land use/cover, which has a great impact on the spatial and temporal distribution of land surface albedo.

Figure 6 shows the spatial distributions in Exp1 and the differences (Exp1 minus Exp2) in the annual average LAI and surface albedo. Figure 6a depicts the LAI gradient from southeast to northwest, while Fig. 6b shows the increased LAI in most part of north China. Figure 6c indicates that surface albedo is small in eastern and southeastern China and high in northern and northwestern China, while Fig. 6d
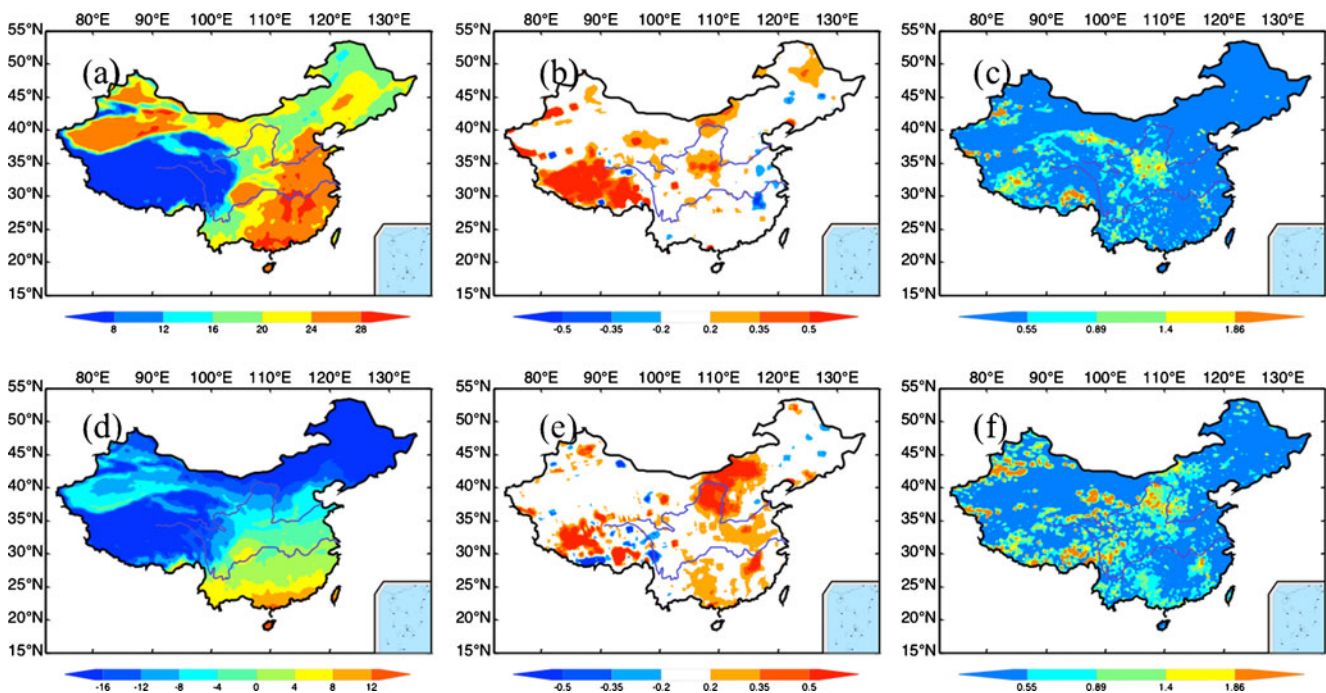
Fig. 5 Spatial distributions of temperature (**a** summer, **c** winter; °C) and temperature change due to LUCC (**b** summer, **d** winter; °C) and *t*-test value at four different confidence levels (*left* to *right*: 70, 80, 90, 95 %) (**c** summer, **f** winter)

shows reduced surface albedo in many areas. In particular, the surface albedo in the Hetao Plain was decreased obviously, which also was the region with the most obvious land use/cover change. Since albedo is defined as the ratio of integrated total reflected solar radiation to the integral of incoming solar radiation, the change of the surface should play a major role in the change of albedo; in the Noah LSM, albedo has a pronounced seasonal variation. When higher albedo occurred, the surface brightened because of increased bare soil; dry and withered vegetation leaves and stems further contributed to higher albedo. Land surface albedo directly controls the net solar radiation absorbed at the surface, and thus it influences the balance of surface energy. Therefore, when albedo is reduced in most areas, the annual mean net short radiant flux (the difference between incoming and outgoing shortwave radiation) increased in most areas. In this study, the most notable change of albedo took place in the Hetao Plain (Fig. 6d). The energy absorbed by the surface is radiated from the Earth's surface as terrestrial longwave radiation. The amount of energy emitted is primarily dependent on the temperature of the surface. The hotter the surface, the more radiant energy it will emit. So, in the Hetao Plain the net longwave also increased (Fig. 7d). The radiation balance of the Earth's system is an accounting of the incoming and outgoing components of radiation. Figure 7f shows that the net radiant flux also increased in the Hetao Plain with an amplitude above 5 Wm^{-2}.

The way heat, moisture, momentum, dust, and pollutants move upward from the surface into the atmosphere is affected by the interactions between land surface and the atmospheric

boundary layer (Weaver and Avissar 2001). A continuous exchange of energy takes place between the Earth's surface and the atmosphere. Based on Verhoef et al. (1999), assuming that horizontal flux divergence and heat storage are insignificant, the net radiation could be dissipated as sensible heat, evaporation (*LE*, where *L* is the latent heat of evaporation and *E* is the evaporation rate), and soil heat fluxes. Figure 8 shows the spatial distribution of sensible heat and latent heat fluxes. Figure 8b indicates that the sensible heat in most areas of eastern China decreased, but it increased most obviously in the Hetao Plain, where the magnitude reached approximately 5 Wm^{-2}. The LUCC made the latent heat flux increase in most areas, but there is an obvious decrease in the middle of the Yangtze River Basin, with maximum amplitude of 2.5 Wm^{-2}. In contrast, the apparent increase occurred in North China (Fig. 8d). This is because latent heat flux is mainly affected by surface water vapor and vegetation transpiration. The sensible heat flux increased in the area where the albedo was reduced; the latent heat flux increased in most areas, which is well in response to the temperature increase.

8 Precipitation and circulation

There are many connections between land surface characteristics and the water cycle. First, the land cover can affect both the degree of infiltration and runoff following precipitation events. Second, the degree of vegetation cover and surface albedo can affect the rates of evaporation, humidity level, and
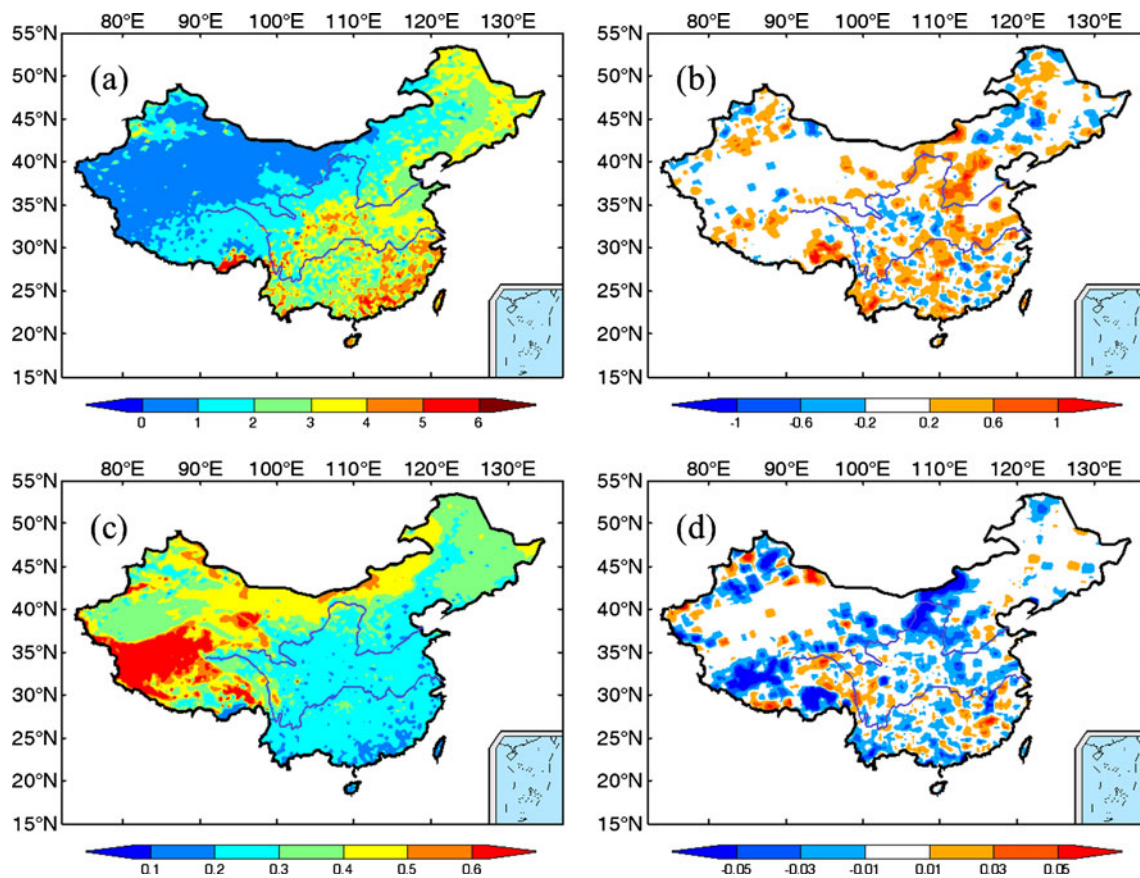
Fig. 6 Spatial distributions of annual mean LAI (**a**) and LAI change due to LUCC (**b**), albedo (**c**), and albedo change (**d**) due to LUCC
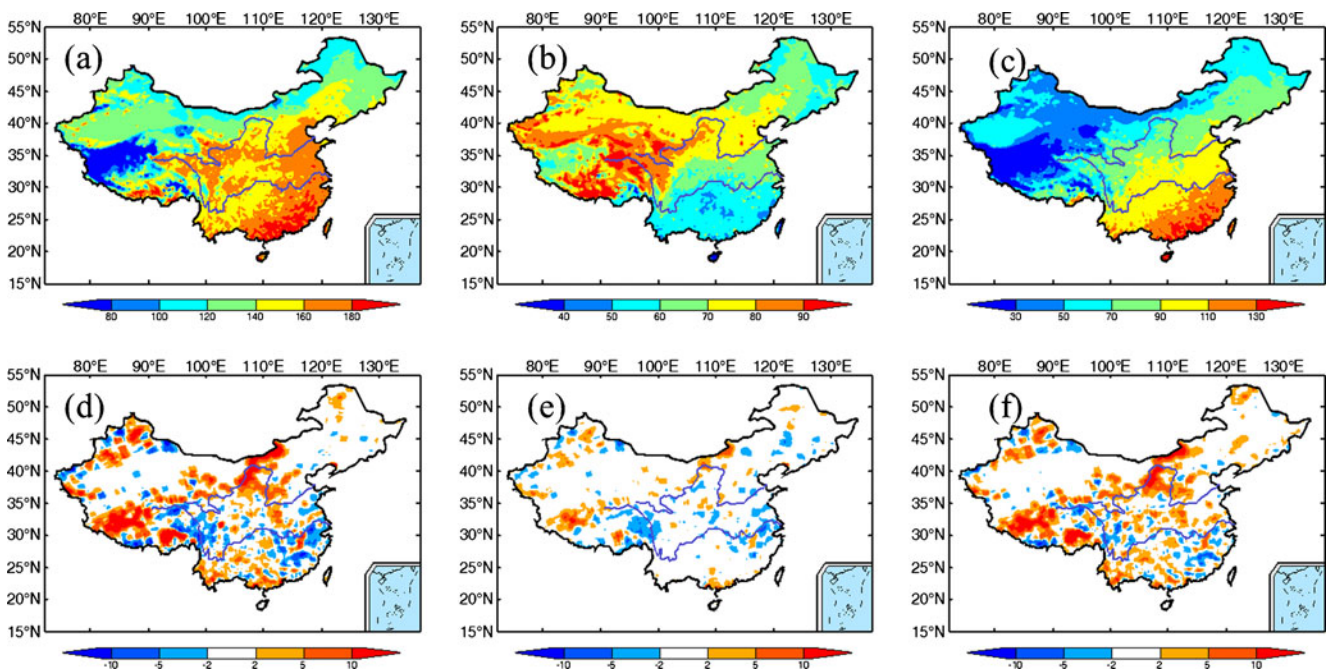

Fig. 7 Spatial distributions of annual mean radiation flux (**a** net shortwave flux, **b** net longwave flux, and **c** net radiation) and their changes due to LUCC (**d–f**), Wm^{-2}
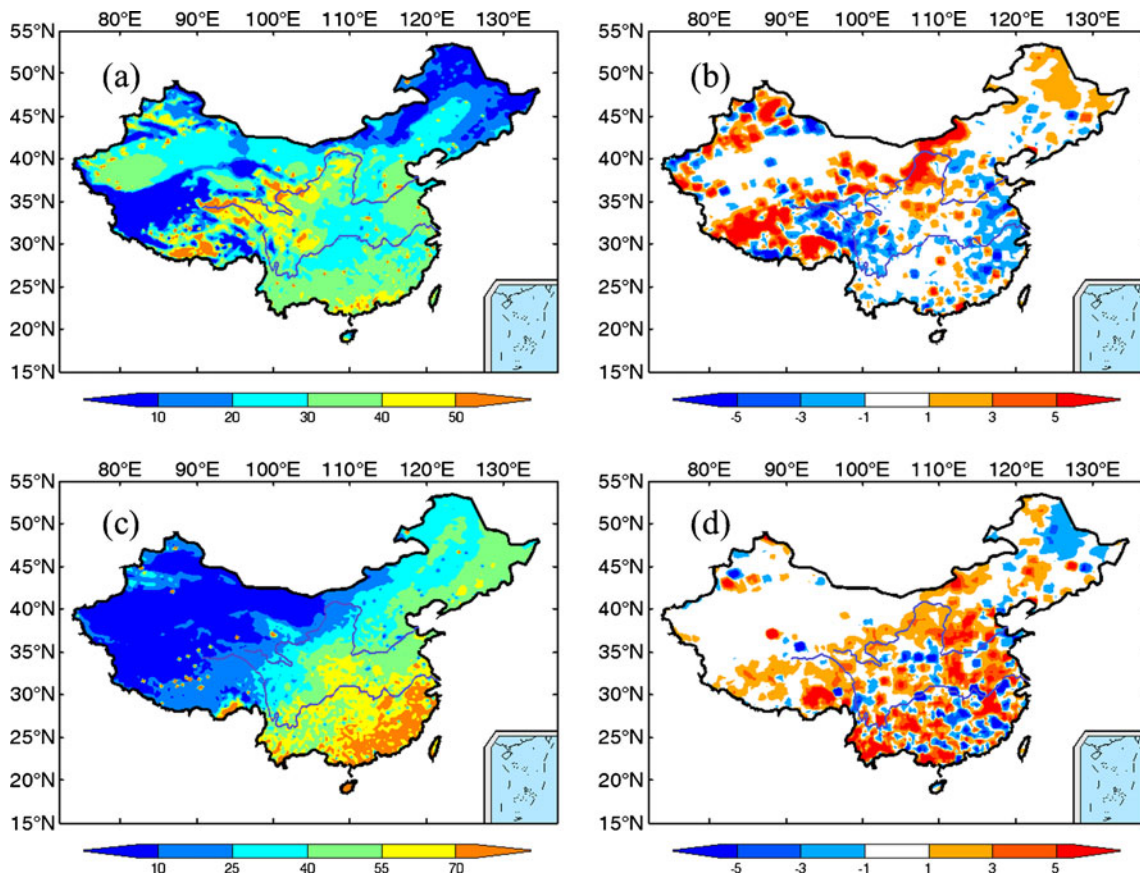
Fig. 8 Spatial distribution of annual mean surface heat flux (**a** sensible heat flux, **c** latent heat flux) and their changes due to LUCC (**b**, **d**), Wm^{-2}

cloud formation. Figure 9 shows the spatial distribution of summer precipitation in Exp1 and the corresponding percentage change between Exp1 and Exp2 (with respect to Exp1) and the *t*-test value in four different confident levels (70, 80, 90, and 95 %). Figure 9b indicates that summer precipitation increased in most of north China, especially in the Hetao Plain, but the *t*-test value (Fig. 9c) shows that the confidence level of precipitation in Hetao Plain is less than 90 %. In the historical record, the mixed land use belt has been sensitive to the global-scale climate changes. The main airflows that bring moisture to the East Asian continent in summer are the Indian

monsoon and South China Sea summer monsoon (Xue 1996). As observed from the wind vector and water vapor transportation at 850 hPa (Fig. 10), when the monsoon flow strengthens, more moisture flux comes from South China, arriving in the Hetao Plain, and the greater east–west thermal gradient, which produced strong northward transport of moisture and cyclone condition (Xue et al., 2004); therefore, the precipitation increased in this area. In North China, especially in the arid and semi-arid regions there, there was an increasing trend of precipitation and an increasing trend of evaporation. The central part of North China is influenced by the northern edge
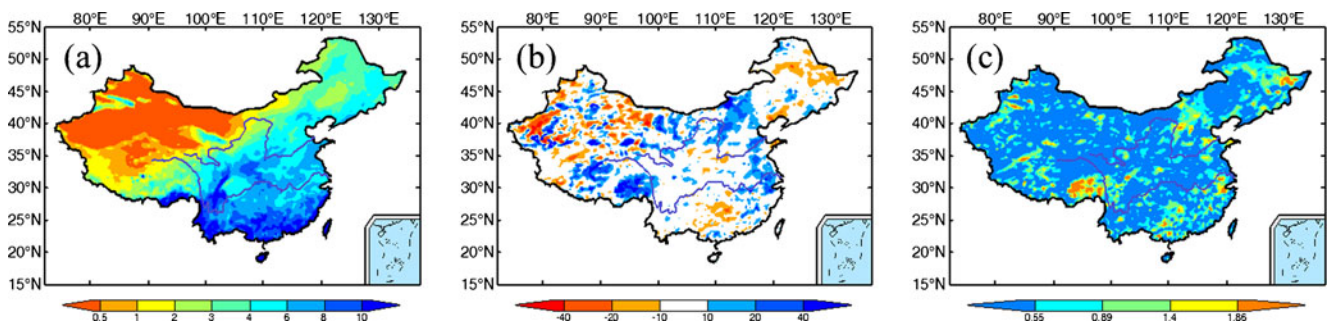

Fig. 9 Spatial distribution of summer mean precipitation (**a** Exp1, mm/day) and percentage change due to LUCC (**b** (Exp2 − Exp1)/Exp1, %) and *t*-test value in four different confidence levels (*left* to *right*: 70, 80, 90, 95 %) (**c**)
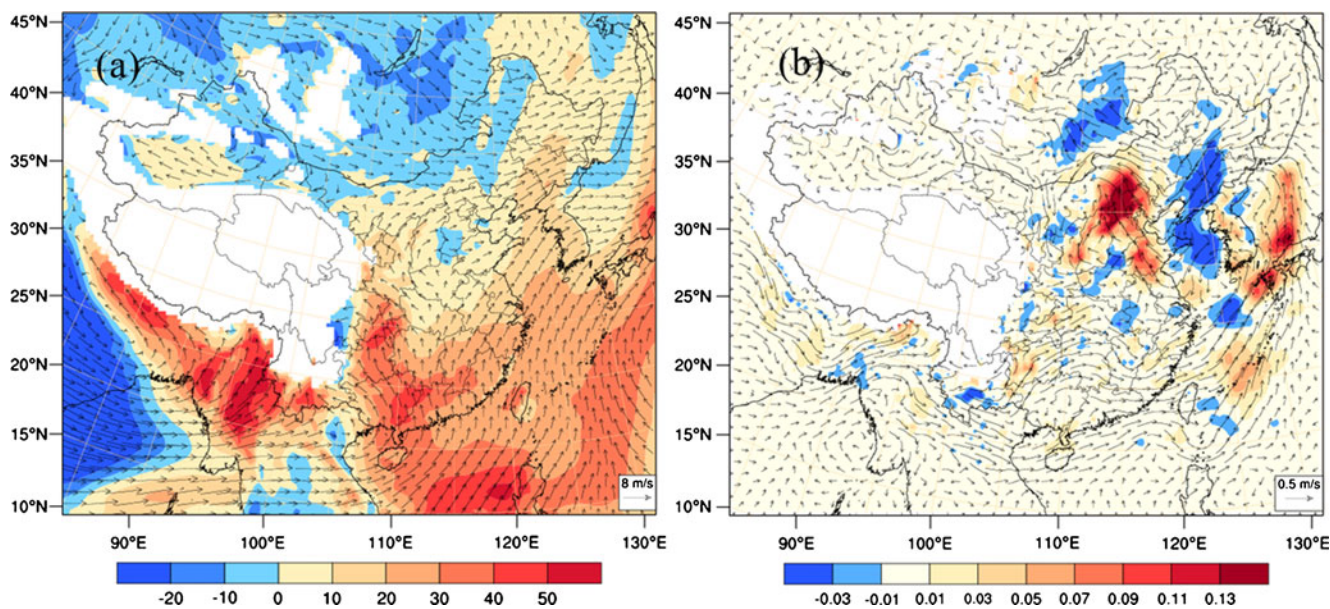
Fig. 10 Wind vector (ms^{-1}) and water vapor transportation (g/kg×m/s) at 850 hPa (**a**) and their changes due to LUCC (**b**)

of the East Asian summer monsoon; thus, the variation of precipitation there is markedly influenced by the variation of the strength of the monsoon.

The vertical wind speed for summer and winter (Fig. 11) over three different sub-regions shows that the lower

atmosphere of the Hetao Plain and Yangtze River Delta had been more impacted by the LUCC in summer than in winter, but an opposite change happened in the Pearl River Delta, where the East Asian monsoon had a more prominent impact. The vertical profile of water vapor mixing ratio for summer (not
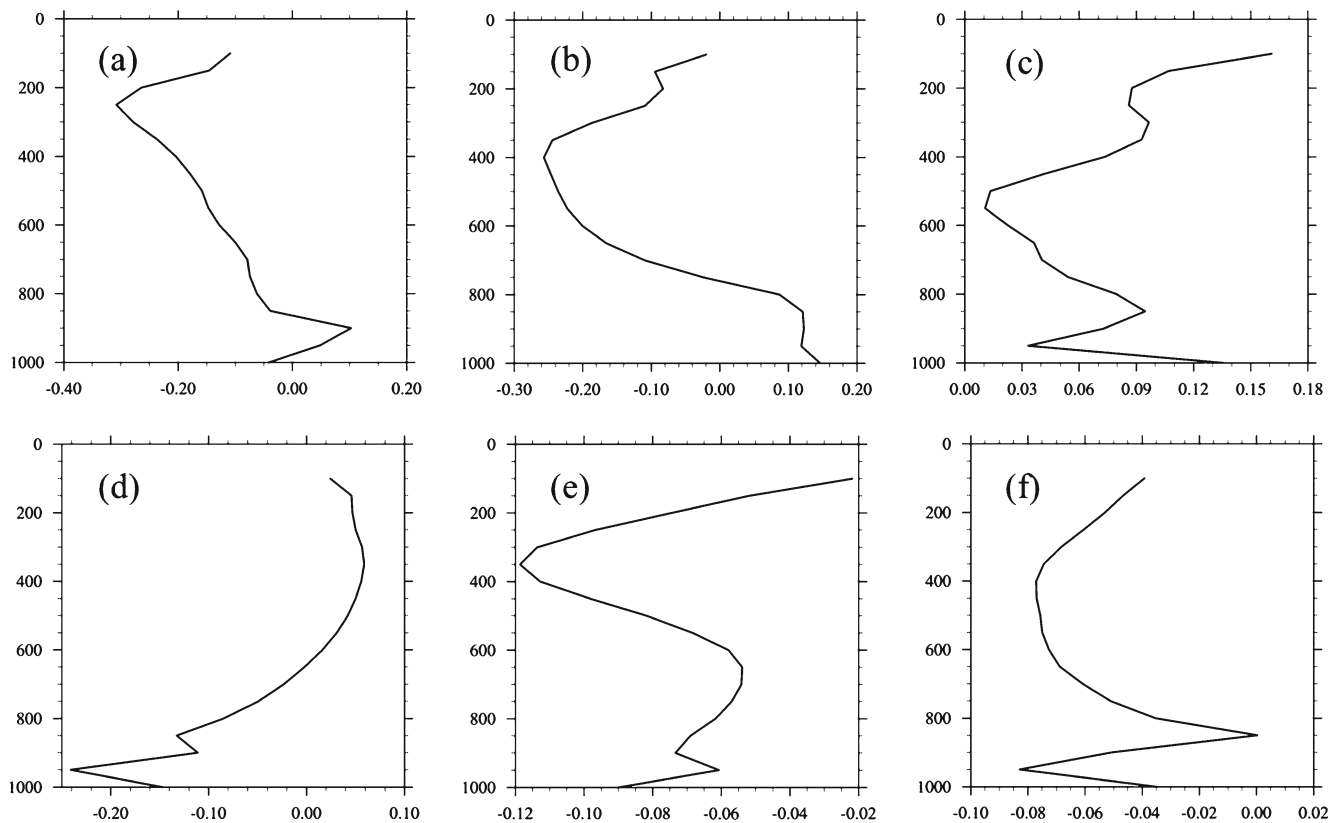

Fig. 11 Vertical profile of wind speed (ms^{-1}) for summer (*top panels*) and winter (*bottom panels*) over different regions due to LUCC: **a**, **d** the Hetao Plain, **b**, **e** the Yangtze River Delta, **c**, **f** the Pearl River Delta

shown) indicates that the most significant change of bottom water vapor caused by LUCC is located in the Hetao Plain.

9 Conclusions and discussion

In the study, using the MODIS land cover products of 2001 and 2008, the WRF model is employed to simulate the influence of the LUCC on regional climate over China from December 2006 to December 2011.

The most obvious change by LUCC in China is in the Hetao Plain, where the former open and closed shrublands had been replaced by the grassland. Based on the WRF physical parameters, the new land cover albedo is less than the old one. In addition, Table 1 shows that the most obvious increasing vegetation is grassland and that the shrublands are decreased apparently. The annual average surface albedo was reduced in most areas due to LUCC, and the most notable place is the Hetao Plain.

Under the scenario of 2001 LUCC and 2008 LUCC, the most obvious increase of summer temperature was in the north and south part of Hetao Plain, with a magnitude of change above 0.35 °C. The most noticeable decrease was located in Yangtze River Basin. Unlike the change of summer temperature, the winter temperature increased in most parts of China, and the most obvious change took place in the Hetao Plain and the north of it. The temperature change was greater in winter than in summer. In the sub-regions, the temperature and precipitation in the Hetao Plain had the same signs of change, and in that of the other two areas (the Yangtze River Delta and the Pearl River Delta) both temperature and precipitation also increased.

The radiation flux, including net shortwave and net radiation, all increased in the Hetao Plain, and the wind field also changed in the Hetao Plain. The LUCC increases latent heat flux in most areas, even with the maximum amplitude of 5 Wm^{-2}. The sensible heat decreased in most parts of eastern China, but the most obvious increase occurred in the Hetao Plain, where the maximum magnitude reached approximately 5 Wm^{-2}.

Summer precipitation increased in most of north China, especially in the Hetao Plain, but the t-test value shows that the confidence level of precipitation in Hetao Plain is less than 90 %.

References

Bonan GB (1997) Effects of land use on the climate of the United States. Clim Chang 37:449–486

Chase TN, Pielke RA, Kittel T, Nemani R, Running SW (1996) Sensitivity of a general circulation model to global changes in leaf area index. J Geophys Res 101:7393–7408

Chen F, Dudhia J (2001) Coupling an advanced land-surface/hydrology model with the Penn State/NCAR MM5 modeling system. Part I: model description and implementation. Mon Wea Rev 129:569–585

Dudhia J (1989) Numerical study of convection observed during the winter monsoon experiment using a mesoscale two-dimensional model. J Atmos Sci 46:3077–3107

Feddema JJ, Oleson KW, Bonan GB, Mearns LO, Buja LE, Meehl GA, Washington WM (2005) The importance of land-cover change in simulating future climates. Science 310:1674–1678

Findell KL, Shevliakova E, Milly PCD, Stouffer RJ (2007) Modeled impact of anthropogenic land cover change on climate. J Climate 20:3621–3634

Friedl MA, McIver DK, Hodges J, Zhang XY, Muchoney D, Strahler AH, Woodcock CE, Gopal S, Schneider A, Cooper A, Baccini A, Gao F, Schaaf C (2002) Global land cover mapping from MODIS: algorithms and early results. Remote Sens Environ 83:287–302

Friedl MA, Sulla-Menashe D, Tan B, Schneider A, Ramankutty N, Sibley A, Huang X (2010) MODIS Collection 5 global land cover: algorithm refinements and characterization of new datasets. Remote Sens Environ 114:168–182

Fuller T, Sanchez-Cordero V, Illoldi-Rangel P, Linaje M, Sarkar S (2007) The cost of postponing biodiversity conservation in Mexico. Biol Conserv 134:593–600

Hodges J (2002) Validation of the consistent-year V003 MODIS land cover product. http://geography.bu.edu/landcover/userguidelc/consistent.htm

Hong SY, Lim JOJ (2006) The WRF Single-Moment 6-Class microphysics scheme (WSM6). J Korean Meteor Soc 42:129–151

Hong S, Noh Y, Dudhia J (2006) A new vertical diffusion package with an explicit treatment of entrainment processes. Mon Weather Rev 134:2318–2341

Issiaka IM, Boubacar Y, Yansheng G (2012) Land-use and land-cover change in semi-arid zone: the case of Waro-Souloulou Area in Goulbi Maradi watershed in the Republic of Niger. Environ Nat Resour Res 2(1):47–62

Kain JS (2004) The Kain-Fritsch convective parameterization: an update. J Appl Meteorol 43:170–181

LaCasse KM, Splitt ME, Lazarus SM, Lapenta WM (2008) The impact of high-resolution sea surface temperatures on the simulated nocturnal Florida marine boundary layer. Mon Weather Rev 136:1349–1372

Lu D, Mausel P, Brondizio E, Moran E (2004) Change detection techniques. Int J Remote Sens 25:2365–2407

Lu LX, Shuttleworth WJ (2002) Incorporating NDVI-derived LAI into the climate version of RAMS and its impact on regional climate. J Hydrometeorol 3:347–362

Ma ZG (2007) The interdecadal trend and shift of dry/wet over the central part of North China and their relationship to the Pacific Decadal Oscillation (PDO). Chinese Sci Bull 52:2130–2139

Mlawer EJ, Taubman SJ, Brown PD, Iacono MJ, Clough SA (1997) Radiative transfer for inhomogeneous atmospheres: RRTM, a validated correlated-k model for the longwave. J Geophys Res 102:16663–16682

Nunes C, Auge, JI (1996) Land use and land cover change (LUCC) implementation strategy. IGBP report no. 48 and IHDP report no. 10.

Pielke RA, Marland G, Betts RA, Chase TN, Eastman JL, Niles JO, Niyogi D, Running SW (2002) The influence of land-use change and landscape dynamics on the climate system: relevance to

climate-change policy beyond the radiative effect of greenhouse gases. Philos T Roy Soc A 360:1705–1719

Pitman AJ, de Noblet-Ducoudre N, Cruz FT, Davin EL, Bonan GB, Brovkin V, Claussen M, Delire C, Ganzeveld L, Gayler V, van den Hurk BJJM, Lawrence PJ, van der Molen MK, Mueller C, Reick CH, Seneviratne SI, Strengers BJ, Voldoire A (2009) Uncertainties in climate responses to past land cover change: first results from the LUCID intercomparison study. Geophys Res Lett 36

Shalaby A, Tateishi R (2007) Remote sensing and GIS for mapping and monitoring land cover and land-use changes in the northwestern coastal zone of Egypt. Appl Geogr 27(1):28–41

Terry LS, Benjamin MS, Kristi LS, Michelle AB, Ryan RR, Stacie LB, Rachel RS, Ronald LK, Zhu Z (2012) Spatially explicit land-use and land-cover scenarios for the Great Plains of the United States. Agric Ecosyst Environ 153:1–15

Tian Y, Dickinson RE, Zhou L, Zeng X, Dai Y, Myneni RB, Knyazikhin Y, Zhang X, Friedl M, Yu II, Wu W, Shaikh M (2004) Comparison of seasonal and spatial variations of leaf area index and fraction of absorbed photosynthetically active radiation from Moderate Resolution Imaging Spectroradiometer (MODIS) and common land model. J Geophys Res 109

Turner BL, David S, and Liu Y (1995) Land use and land cover change science/research plan. IHDP report no. 07

Verhoef A, Allen SJ, Lloyd CR (1999) Seasonal variation of surface energy balance over two Sahelian surfaces. Int J Climatol 19:1267–1277

Weaver CP, Avissar R (2001) Atmospheric disturbances caused by human modification of the landscape. B Am Meteorol Soc 82:269–281

WCS, CISCIN (2002) http://www.wcs.org/&http://www.ciesin.columbia.edu/

Xue YK, Fennessy MJ, Sellers PJ (1996) Impact of vegetation properties on US summer weather prediction. J Geophys Res 101:7419–7430

Xue Y (1996) The Impact of desertification in the Mongolian and the Inner Mongolian grassland on the regional climate. J Climate 9:2173–2189

Xue Y, Juang H-MH, Li W, Prince S, DeFries R, Jiao Y, Vasic R (2004) Role of land surface processes in monsoon development: East Asia and West Africa. J Geophy Res 109:D03105. doi:10.1029/2003JD003556

Zhao M, Pitman AJ, Chase T (2001) The impact of land cover change on the atmospheric circulation. Clim Dynam 17:467–477